Cell Reports

Experience-dependent plasticity modulates ongoing activity in the antennal lobe and enhances odor representations

Graphical abstract

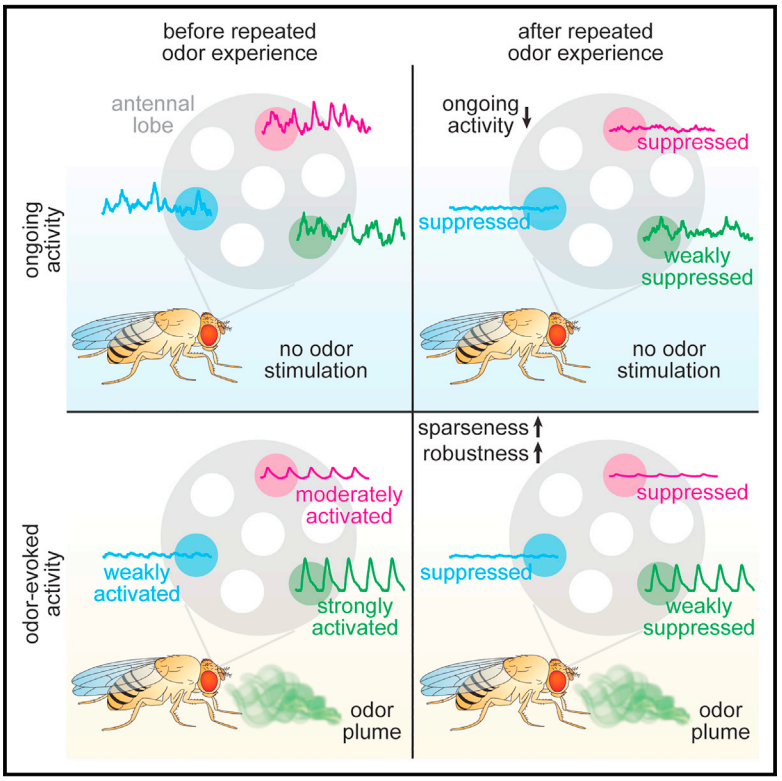

Highlights

- The fruit fly antennal lobe exhibits spatiotemporally organized ongoing activity
- Repeated odor experience decreases the amplitude and number of ongoing calcium events
- Odor experience enhances the robustness and the specificity of odor representations
- Representations of different odors become more dissimilar upon repeated exposure

Authors

Luis M. Franco, Emre Yaksi

Correspondence

luis.franco@lifesci.ucsb.edu (L.M.F.), emre.yaksi@ntnu.no (E.Y.)

In brief

Franco and Yaksi show that ongoing activity in the *Drosophila melanogaster* antennal lobe is spatiotemporally organized. Importantly, repeated odor experience decreases the amplitude and number of calcium events in glomerular ongoing activity, and enhances the robustness, specificity, and discriminability of odor representations.

Franco & Yaksi, 2021, Cell Reports *37*, 110165
December 28, 2021 © 2021 The Author(s).
https://doi.org/10.1016/j.celrep.2021.110165

Cell Reports

CellPress
OPEN ACCESS

Report

Experience-dependent plasticity modulates ongoing activity in the antennal lobe and enhances odor representations

Luis M. Franco[1,2,3,*] and Emre Yaksi[1,4,5,*]
[1]Neuroelectronics Research Flanders (NERF), KU Leuven, Leuven 3001, Belgium
[2]VIB Center for the Biology of Disease, KU Leuven, Leuven 3000, Belgium
[3]Neuroscience Research Institute, University of California, Santa Barbara, Santa Barbara, CA 93106, USA
[4]Kavli Institute for Systems Neuroscience and Centre for Neural Computation, NTNU, Trondheim 7030, Norway
[5]Lead contact
*Correspondence: luis.franco@lifesci.ucsb.edu (L.M.F.), emre.yaksi@ntnu.no (E.Y.)
https://doi.org/10.1016/j.celrep.2021.110165

SUMMARY

Ongoing neural activity has been observed across several brain regions and is thought to reflect the internal state of the brain. Yet, it is important to understand how ongoing neural activity interacts with sensory experience and shapes sensory representations. Here, we show that the projection neurons of the fruit fly antennal lobe exhibit spatiotemporally organized ongoing activity. After repeated exposure to odors, we observe a gradual and cumulative decrease in the amplitude and number of calcium events occurring in the absence of odor stimulation, as well as a reorganization of correlations between olfactory glomeruli. Accompanying these plastic changes, we find that repeated odor experience decreases trial-to-trial variability and enhances the specificity of odor representations. Our results reveal an odor-experience-dependent modulation of ongoing and sensory-evoked activity at peripheral levels of the fruit fly olfactory system.

INTRODUCTION

Brain circuits display continuous fluctuations of neural activity, even in the absence of sensory stimuli or environmental alterations. This ongoing neural activity is widespread in the brain, spanning from sensory systems to higher brain regions, and it has been associated with various cognitive functions (Raichle, 2010; Sadaghiani et al., 2010). Despite being previously considered noise, ongoing neural activity is highly structured, often exhibiting spatiotemporally organized patterns (Arieli et al., 1996; Bartoszek et al., 2021; Fore et al., 2020; Fox et al., 2005; Jetti et al., 2014; Marques et al., 2020; Romano et al., 2015; Shimaoka et al., 2019), reflecting the functional connectivity and internal states of neural networks (Andalman et al., 2019; Lange and Haefner, 2017; Lovett-Barron et al., 2017). Moreover, accumulating evidence indicates that continuous interactions between externally driven sensory representations and internally generated ongoing activity shape each other. For instance, during specific tasks, ongoing neural activity is transiently suppressed across the human cortex, except in regions engaged in the task (Raichle, 2010; Raichle et al., 2001). Similarly, sensory-driven transient changes in ongoing activity have been observed in several brain regions across different species (Galán et al., 2006a; Hahn et al., 2012; Ichinose et al., 2017; Romano et al., 2015; Shimaoka et al., 2019; Vanni and Murphy, 2014; Wosniack et al., 2021). Interestingly, repeated exposure to sensory stimuli can also lead to long-term experience-dependent alterations in neural circuit connectivity and activity. Such experience-dependent alterations have been shown to stabilize neuronal responses to behaviorally relevant sensory stimuli, and even enhance stimulus discriminability (Bazhenov et al., 2005; Bhandawat et al., 2007; Galán et al., 2006b; Jacobson et al., 2018; Kilgard and Merzenich, 1998; Musall et al., 2019; Poort et al., 2015; Stopfer and Laurent, 1999).

In the olfactory system, ongoing activity in the absence of odor stimulation is reported from the level of olfactory sensory neurons (Bhandawat et al., 2007; Friedrich and Laurent, 2004; Nagel et al., 2015; Olsen et al., 2010) to the olfactory bulbs (Fujimoto et al., 2019; Galán et al., 2006b; Gorin et al., 2016; Nagel and Wilson, 2016; Padmanabhan and Urban, 2010) and the olfactory cortex (Lottem et al., 2016; Popov and Szyszka, 2020; Rojas-Líbano et al., 2014; Wilson and Yan, 2010). To some extent, this ongoing activity can be interpreted as background noise, which is generated by the internal biophysical properties of neurons at each level (Kazama and Wilson, 2009; Padmanabhan and Urban, 2010). However, evidence from the vertebrate olfactory bulb (Gorin et al., 2016; Padmanabhan and Urban, 2010) and the honeybee antennal lobe (Galán et al., 2006b) suggests that ongoing neural activity reflects the structured synchronous activity of neuronal ensembles in the olfactory system. Moreover, top-down modulation of olfactory bulb inhibitory interneurons is known to modulate not only sensory responses, but also the resting state of ongoing activity in olfactory circuits (Bundschuh et al., 2012; Dacks et al., 2009; Liu, 2020; Lottem et al., 2016; Petzold et al., 2009). In fact, sensory experience is known to play an important role in

This is an open access article under the CC BY-NC-ND license (http://creativecommons.org/licenses/by-nc-nd/4.0/).

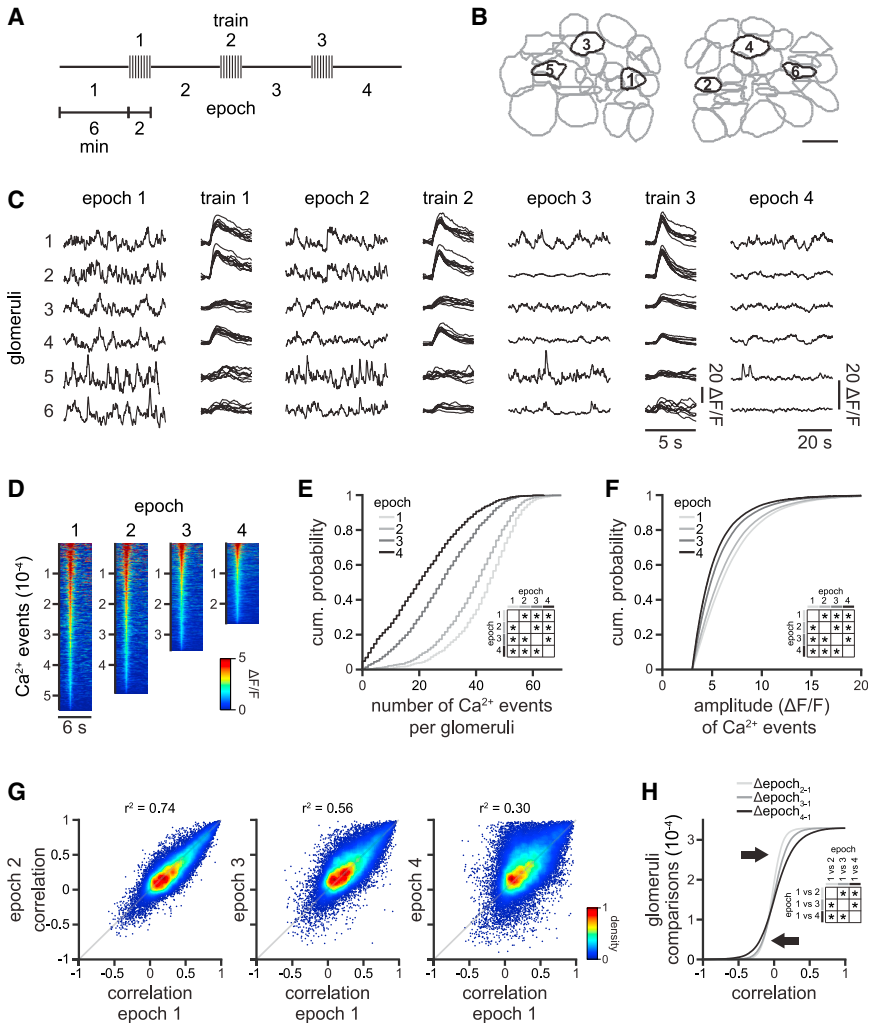

Figure 1. Repetitive odor exposure reduces ongoing activity in the antennal lobe

(A) Experimental design consisting of 3 trains of 8 odor repetitions interleaved by 4 epochs of ongoing activity. Eight different odors were tested. See STAR methods for details.

(B and C) Example of glomerular locations (B), their ongoing activity traces, recorded in between odor stimulations, and their odor-evoked responses to amyl acetate, obtained in stimulation trains (C). Scale bar, 10 μm.

(D) Heatmaps of all detected calcium events across the 4 ongoing activity epochs. Events are sorted based on their amplitude, from highest (top) to lowest (bottom). Note that the number of calcium events decreases across epochs.

(E and F) The number (E; epoch 1 vs 2, $p = 7.2 \times 10^{-21}$; epoch 1 vs 3, $p = 2.3 \times 10^{-187}$; epoch 1 vs 4, $p = 0$; epoch 2 vs 3, $p = 1.7 \times 10^{-101}$; epoch 2 vs 4, $p = 7.5 \times 10^{-227}$; epoch 3 vs 4, $p = 5.3 \times 10^{-39}$F; epoch 1 vs 2, $p = 2.9 \times 10^{-9}$; epoch 1 vs 3, $p = 5.4 \times 10^{-82}$; epoch 1 vs 4, $p = 7.6 \times 10^{-150}$; epoch 2 vs 3, $p = 1.1 \times 10^{-40}$; epoch 2 vs 4, $p = 1.1 \times 10^{-93}$; epoch 3 vs 4, $p = 8.9 \times 10^{-16}$) of ongoing calcium events progressively and significantly decreased after trains of odor stimulation.

(G) Pearson's correlations of ongoing activity among all glomeruli compared across epochs.

(H) Cumulative distribution of the change in Pearson's correlations of ongoing activity (n = 32,947 glomerulus pairs; Δepoch2–1 vs Δepoch3–1, $p = 7.8 \times 10^{-202}$; Δepoch2–1 vs Δepoch4–1, $p = 0$; Δepoch3–1 vs Δepoch4–1, $p = 1.7 \times 10^{-64}$).

Statistical comparisons: linear mixed-effects model, fixed effect for epoch, random effects for fly and odor (n = 1,268 glomeruli in 24 flies).

See also Figures S1 and S2.

modulating olfactory representations and synchrony across multiple levels of the olfactory pathway (Galán et al., 2006b; Jacobson et al., 2018; Rojas-Líbano et al., 2014). Yet, the link between the experience-dependent plasticity of odor representations and ongoing neural activity is not fully understood.

In this study, we show that the projection neurons of the fruit fly antennal lobe exhibit spatiotemporally organized ongoing activity in the absence of odor stimulation. We also find that, upon repeated odor exposure, the amplitude and number of calcium events occurring during periods of ongoing neural activity decrease, resulting in alterations in correlations between olfactory glomeruli. Moreover, this experience-dependent plasticity decreases trial-to-trial variability of odor representations, thereby increasing the robustness and specificity of olfactory computations.

RESULTS

To investigate the spatial and temporal features of ongoing activity in the *Drosophila melanogaster* antennal lobe, we measured calcium signals in ;GH146-Gal4/UAS-GCaMP6m; +/+ fruit flies expressing the calcium indicator GCaMP6m in the projection neurons of the antennal lobe (Figure 1A). We evaluated the impact of repeated odor exposure on the ongoing activity of the antennal lobe by applying 3 trains of 8 consecutive stimuli with the same odor, interleaved by epochs of 6-min-long ongoing activity (Figures 1A–1C). Eight different odors (1-pentanol, 2-heptanone, 3-octanol, 4-methylcyclohexanol, amyl acetate, benzaldehyde, ethyl acetate, and ethyl valerate) were used in separate experiments. Individual olfactory glomeruli were detected (Figures 1B and 1C) using an independent component analysis (Franco et al., 2017; Mukamel et al., 2009). We observed that the number and the amplitude of calcium events significantly decreased across epochs after repeated odor exposure (Figures 1D–1F and S1), which was consistent across all tested odors (Figures S1A and S1D). While changes in ongoing activity were significant across epochs (Figures S1B and S1E), we observed little or no change in the number and amplitude of ongoing calcium events within each epoch (Figures S1C and S1F). This reduction of ongoing glomerular activity was accompanied by a redistribution of pairwise correlations between individual glomeruli (Figures 1G and 1H), indicating a functional reorganization of the antennal

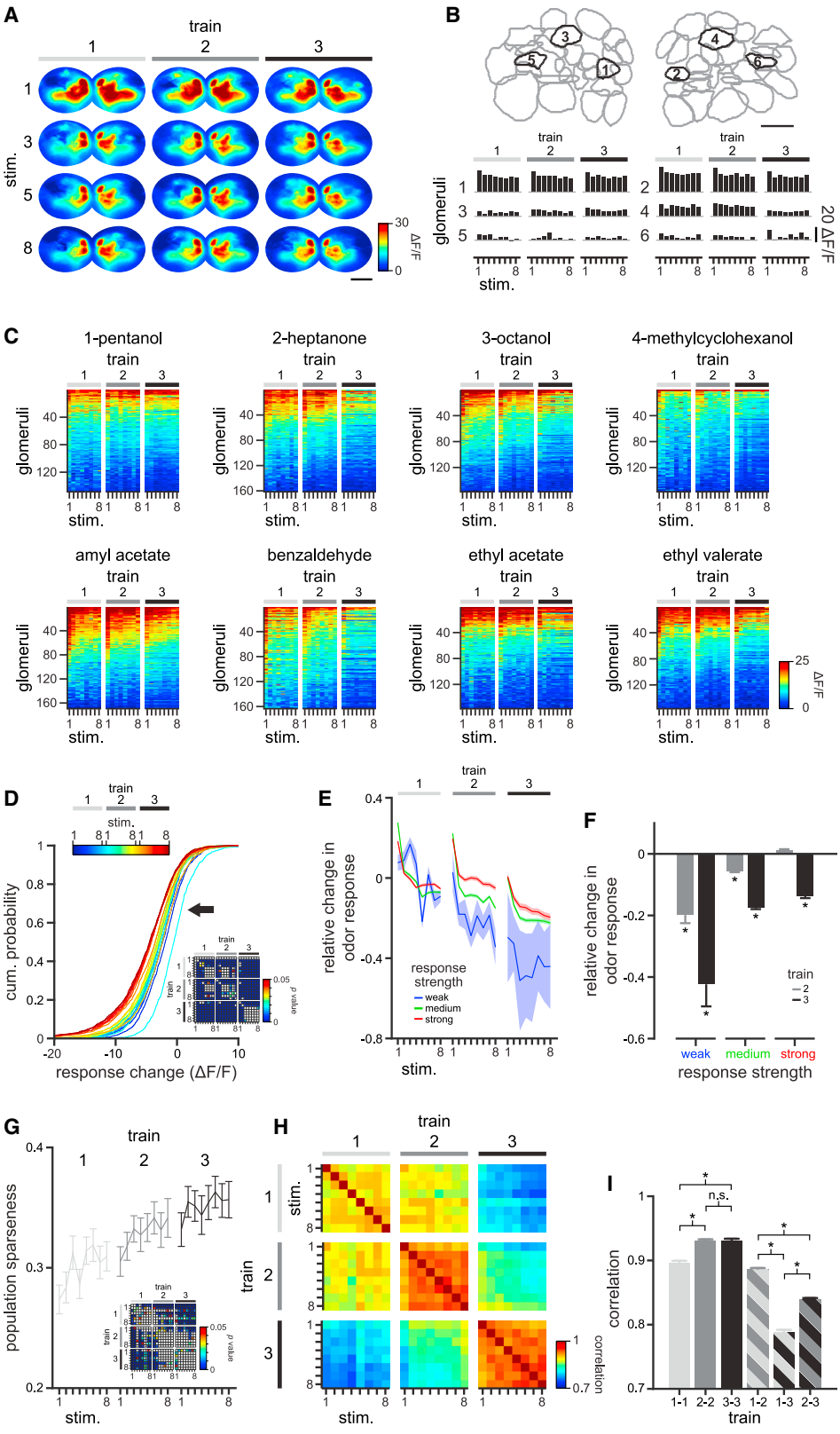

(legend on next page)

lobe. Furthermore, we observed that functional clusters of olfactory glomeruli were stable across all epochs of ongoing activity, where pairs of olfactory glomeruli remained in their respective k-means clusters (Figure S2). These results indicate a significant, gradual, and cumulative experience-dependent modulation of the ongoing activity in *Drosophila* antennal lobe circuits upon repeated odor exposure.

Next, we asked whether repeated odor exposure, modulating ongoing glomerular activity, can also lead to alterations in odor representations. We observed a gradual reduction in odor responses upon exposure to each train of odor stimuli (Figures 2A–2D and S3). However, glomeruli with the largest odor responses tended to remain stable, or even slightly increase their odor responses (Figures 2C and S3A, glomeruli on the top). Conversely, glomeruli with moderate or weaker odor responses showed a reduction in their responses upon repeated odor experience (Figures 2C and S3A, glomeruli in the middle or at the bottom). This was consistent across all tested odors (Figures 2C and S3C). To further quantify this, we categorized olfactory glomeruli based on their odor response amplitude. For each fly, glomeruli that responded 1 standard deviation below the average response were considered weak or nonresponsive, and glomeruli that responded 1 standard deviation above the average response were considered strongly responsive. All other glomeruli were considered mediumly responsive. We find that repetitive odor exposure significantly increases the number of weakly responsive (or silent) and mediumly responsive glomeruli (Figures 2E and 2F, shown in blue and green). By contrast, strongly responsive glomeruli did not reduce their responses after the first and second trains of stimulation, but only during the third train of stimulation (Figures 2E and 2F, shown in red). Importantly, we also observed a significant relationship between the reduction of odor responses and the reduction of ongoing activity on a glomerulus-by-glomerulus basis (Figure S4).

We hypothesized that such reorganization of glomerular responses may lead to an experience-dependent sparsening of odor representations, where repeated exposure to odors gradually silences most glomeruli, except few specific and strongly responding glomeruli. To quantify this, we measured the population sparseness of glomerular activity patterns, which is equal to 1 if only a single specific glomerulus responds to an odor and is equal to 0 if all glomeruli equally respond to a given odor. We observed a significant, gradual, and cumulative increase in population sparseness upon exposure to each train of odor stimuli (Figures 2G and S5). We expected that this experience-dependent sparsening of odor responses could lead to more robust odor representations, with reduced trail-to-trial variability. To quantify this, we calculated the pairwise similarities of repeated odor representations using Pearson's correlations (Figures 2H and S6) and Euclidean distances (Figure S7). Both methods revealed a significant decrease in trial-to-trial variability (Figures 2I, S6, and S7), enhancing the robustness of odor representations upon repeated odor exposure. This was consistent across all tested odors (Figures S5–S7). Altogether, our results indicate that the antennal lobe circuit gradually undergoes experience-dependent plasticity upon repeated odor exposure, reducing neural noise and trial-to-trial variability, thereby improving the specificity of odor representations.

One possible consequence of the observed experience-dependent increase in the specificity of odor representations is a potential improvement of odor discriminability. To test this, we compared the odor response patterns of 2 different odors, before and after exposing the antennal lobe circuits to repeated stimulation with only 1 of the odors (Figure 3A). Similar to our previous results (Figures 1 and 2), we find that even a short train with 5 odor repetitions led to alterations in both glomerular odor responses and ongoing activity (Figures 3B–3G and S8). Namely, we observed a decrease in the number and amplitude of calcium events, as well as in correlations in ongoing glomerular activity (Figures 3C, 3D, and S8A–S8H). Accompanying these changes, we observed that glomerular responses to the repeated odor became more different from the responses to the unrepeated

Figure 2. Repetitive odor stimulation increases reliability of odor representations

(A) Representative responses to amyl acetate calculated by the percent change of fluorescence intensity (ΔF/F) during 1.5 s after response onset. Scale bar, 20 μm.

(B) Example of glomerular locations (top), and their corresponding odor-evoked responses to amyl acetate (bottom). Scale bar, 10 μm.

(C) Odor responses (averaged over a 1.5-s window after odor onset) for all individual glomeruli across the 3 trains of 8 stimulus repetitions (3 flies per odor). Glomeruli are sorted from the strongest (top) to the weakest (bottom) responding. Odors are indicated above each panel.

(D) Cumulative distribution of the change in odor responses, compared with the first response. Repetitive stimulation progressively and significantly decreases glomerular responses. The arrow highlights the reduction in odor responses.

(E) Average change in odor responses (mean ± standard error of the mean) for all glomeruli that exhibit weak (1 standard deviation [SD] below the mean), strong (1 SD above the mean) and medium (remaining) odor responses, compared with the mean response in the first train. Note that strong responses stay relatively stable for the first 2 trains, decreasing only during the third train. Conversely, medium and weak responses decrease progressively.

(F) Average change in weak, medium, and strongly responding glomeruli (mean ± standard error of the mean). Weak and mediumly responding glomeruli decrease their responses over the second and third trains ($weak_{train1}$ vs $weak_{train2}$, $p = 7.0 \times 10^{-11}$; $weak_{train1}$ vs $weak_{train3}$, $p = 6.2 \times 10^{-9}$; $medium_{train1}$ vs $medium_{train2}$, $p = 3.5 \times 10^{-37}$; $medium_{train1}$ vs $medium_{train3}$, $p = 1.5 \times 10^{-285}$). By contrast, strongly responding glomeruli do not decrease their responses in the second train, with only a small but significant decrease in the third train ($strong_{train1}$ vs $strong_{train3}$, $p = 1.5 \times 10^{-86}$).

(G) Population sparseness significantly increases with repetitive stimulation (mean ± standard error of the mean), indicating a more specific recruitment of a small number of glomeruli upon odor stimulation.

(H) Average pairwise correlations among odor representations elicited in the 3 trains of odor stimuli.

(I) Correlations (mean ± standard error of the mean) among odor representations within (train 1 vs 2, $p = 3.6 \times 10^{-27}$; train 1 vs 3, $p = 5.2 \times 10^{-25}$; train 2 vs 3, $p = 0.8159$) and across (trains 1 and 2 vs 1 and 3, $p = 3.4 \times 10^{-207}$; trains 1 and 3 vs 2 and 3, $p = 4.4 \times 10^{-67}$; trains 1 and 2 vs 2 and 3, $p = 2.1 \times 10^{-71}$) stimulus trains. Representations become significantly more robust after repetitive stimulation.

Statistical comparisons: linear mixed-effects model, fixed effect for train, random effects for fly and odor (n = 1,268 glomeruli in 24 flies). stim., stimulus; n.s., not significant.

See also Figures S3, S4, S5, S6, and S7.

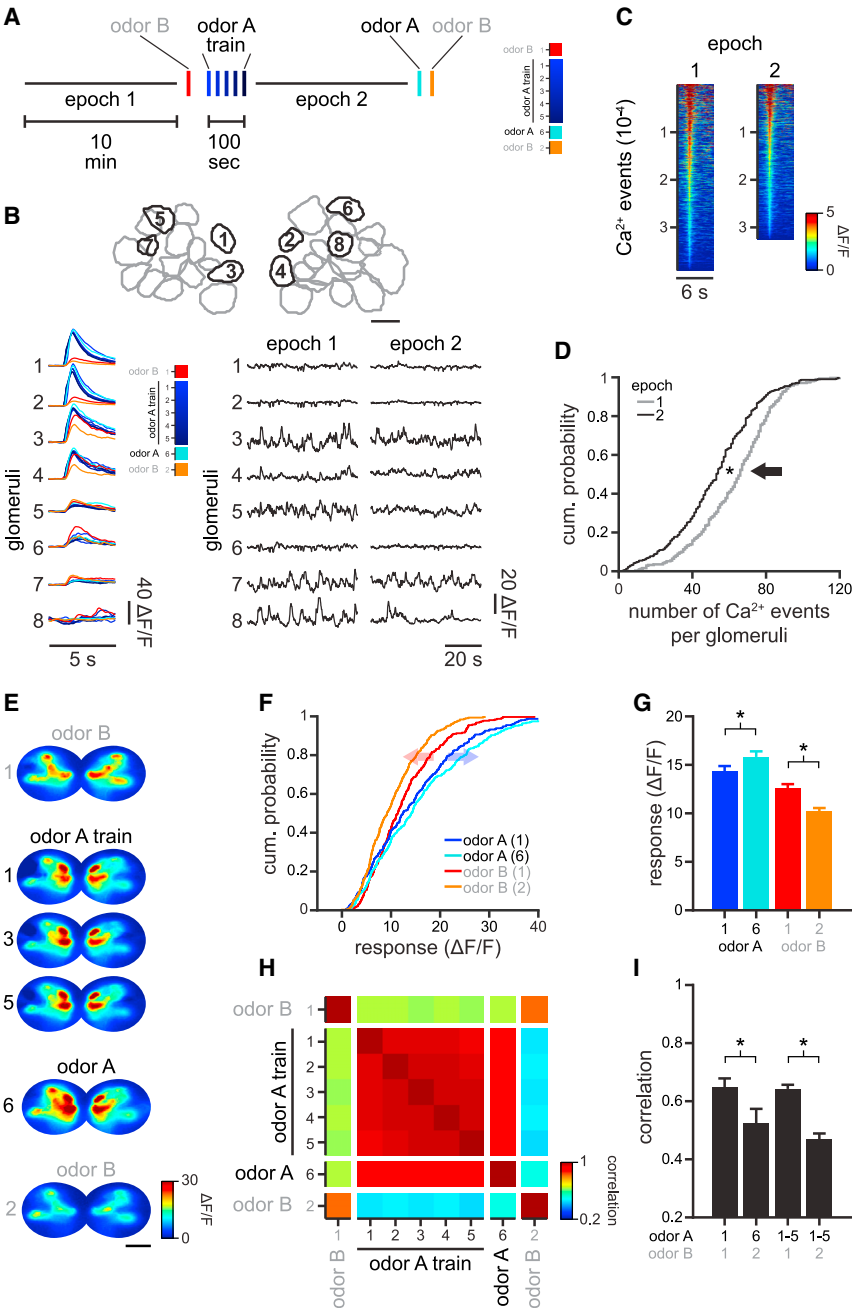

Figure 3. Repetitive odor exposure facilities discrimination of odor representations

(A) Experimental design consisting of 1 train of 5 odor stimuli (blue) preceded by 1 stimulus with a naive odor (red). After a 10-min epoch of ongoing activity, both odors are presented again (cyan and orange).

(B) Examples of the location of glomeruli (top), their corresponding odor-evoked responses (colored traces), and ongoing activity traces recorded during epochs in between odor stimulations. Scale bar, 10 μm.

(C) Heatmaps of all detected calcium events across the 2 ongoing activity epochs. Events are sorted based on their amplitude, from highest (top) to lowest (bottom).

(D) Cumulative distribution of the number of calcium events. Note that the number of calcium events decrease with repetitive stimulation (epoch 1 vs 2, $p = 6.0 \times 10^{-10}$).

(E) Odor maps calculated by the percent change of fluorescence intensity (ΔF/F) over a 1.5-s window after response onset. Scale bar, 20 μm.

(F) Cumulative distribution of glomerular responses for the first and last exposure to odor A and B, respectively. Note that responses to the unrepeated odor B decrease (red arrow), whereas responses to the repeated odor A increase (blue arrow). cum., cumulative.

(G) Odor responses (mean ± standard error of the mean) to the repeated odor A significantly increased after repetitive stimulation (odor A1 vs A6, $p = 0.0437$), whereas responses to the unrepeated odor B significantly decreased (odor B1 vs B2, $p = 3.2 \times 10^{-7}$).

(H) Average pairwise correlations among odor representations elicited by the repeated odor A, and unrepeated odor (B).

(I) Correlations (mean ± standard error of the mean) among odor representations for the repeated odor A and the unrepeated odor (odor B). Note that the representations of the repeated odor A become more different from that of the unrepeated odor B (odors A1–B1 vs odors A6–B2, $p = 0.0054$; odors A1-5-B1 vs odors A1-5-B2, $p = 7.9 \times 10^{-16}$).

Statistical comparisons: linear mixed-effects model, fixed effect for epoch (C), stimulation (G) or correlation (I), random effect for fly (n = 310 glomeruli in 10 flies).

See also Figure S8.

odor, even after 10 min of ongoing activity with no odor stimulation (Figures 3E–3G). In addition, we compared the similarities of odor representations between these 2 odors, before and after repeated exposure to 1 of the odors, by using Pearson's correlations (Figures 3H and 3I) and Euclidean distances (Figures S8I–S8J). All analyses confirmed that the representation of 2 different odors becomes more dissimilar, and thus easier to discriminate upon repeated exposure to only 1 of the odors. Together, these results show that experience-dependent alterations in the antennal lobe improve odor discriminability upon repeated odor exposure.

DISCUSSION

In this study, we showed that the projection neurons of the fruit fly antennal lobe display structured ongoing activity. We also showed that repeated odor exposure triggers experience-dependent plasticity in the antennal lobe, decreasing ongoing activity levels. This, in turn, facilitates more robust odor representations, with reduced trial-to-trial variability and increased odor specificity. Our observations in fruit flies are in line with previous findings of structured ongoing activity in honeybees (Galán et al., 2006b), as well as experience-dependent plasticity of odor

representations in locusts (Bazhenov et al., 2005; Stopfer and Laurent, 1999). Yet, our results tie these previous findings from different insect species and highlight the relationship between sensory representations and ongoing activity in the antennal lobe. Moreover, our results indicate that experience-dependent plasticity extends beyond a few seconds after odor exposure, outlasts the slow kinetics of calcium signals (Chen et al., 2013), can last up to 10 min, and accumulates across 30 min. We argue that repeated odor experience at such time scales is particularly relevant for understanding neural computations underlying olfactory-guided behaviors. When animals navigate across odor plumes, they often encounter not only a single continuous odor pulse, but rather experience repeated odor pulses with dynamically changing exposure frequency (Boie et al., 2018; Lewis et al., 2020; Louis et al., 2008; Park et al., 2016; Porter et al., 2007; Reiten et al., 2017; Van Breugel and Dickinson, 2014; Vickers et al., 2001; Victor et al., 2019). Hence, repeated odor exposure, as we investigated in this study, is likely a common way for animals to experience odor plumes in nature. We argue that the experience-dependent enhancement of odor representations observed upon repeated odor exposure may serve as an important function during odor-guided navigation by adjusting internally generated dynamics (i.e., ongoing activity) of the antennal lobe circuit.

We observed that odor-experience-dependent plasticity dampens ongoing activity fluctuations and reduces the internal noise of the antennal lobe. Indeed, our results showed that those glomeruli with the largest alterations in ongoing activity are also the same glomeruli that exhibit the largest levels of experience-dependent plasticity in odor representations. We also observed that odor experience does not modulate the responses of all glomeruli equally. Instead, glomeruli with strong odor responses remained unaltered (or even slightly amplified), but glomeruli with weak odor responses gradually reduce their responses (Figures 2C–2F and S3). This phenomenon led to a sparsening of odor representations, by preserving the responses of a few glomeruli with strong odor responses and inhibiting the odor responses of the remaining weakly responsive glomeruli. This, in turn, increases the specificity and robustness of odor representations. A potential mechanism for such plasticity may rely on a gradual recruitment of inhibitory local interneurons (LNs) of the antennal lobe. A large fraction of LNs are inhibitory (Berck et al., 2016; Chou et al., 2010; Nagel et al., 2015; Olsen et al., 2010; Sachse et al., 2007), regulating the activity of projection neurons (Franco et al., 2017; Grabe et al., 2020; Wilson and Laurent, 2005) and olfactory receptor neuron terminals (Olsen and Wilson, 2008; Root et al., 2008). Thus, it is likely that repeated odor exposure gradually increases the activity of inhibitory LNs, leading to accumulating levels of the inhibitory neurotransmitter gamma-aminobutyric acid in the antennal lobe. Such recruitment of inhibitory LNs has been previously shown during odor habituation (Das et al., 2011) and in oscillations of activity during odor learning (Bazhenov et al., 2005; Stopfer and Laurent, 1999). Our results suggest that this cumulative buildup of inhibition might in turn lead to a persistent dampening of ongoing activity, reducing noise levels for extended periods of time, beyond the transient odor exposure. Such inhibition, mediated by interneurons, is preserved across the vertebrate olfactory bulb (Abraham et al., 2010; Arevian et al., 2008; Tabor et al., 2008) and may also serve similar purposes. However, we do not rule out the possibility of other plasticity mechanisms that might jointly underlie the alterations that we observe here. Future studies benefiting from the extensive genetic toolbox of fruit flies could further dissect these mechanisms.

Recent studies have demonstrated strong and lasting neuromodulatory control of inhibitory interneurons in the vertebrate olfactory bulb via dopaminergic (Banerjee et al., 2015; Bundschuh et al., 2012; Hsia et al., 1999) and serotonergic (Brill et al., 2016; Dugué and Mainen, 2009; Petzold et al., 2009) modulation. Interestingly, the *Drosophila* neuromodulator octopamine is known to regulate inhibitory LNs in the antennal lobe (Rein et al., 2013), and to influence the internal state of the fly during odor-guided behaviors, such as searching for appropriate food sources (Christiaens et al., 2014) depending on the current nutritional demands (Corrales-Carvajal et al., 2016). Hence, it is possible that repeated odor exposure entrains these neuromodulatory systems, leading to lasting and more effective inhibition in the olfactory bulb and antennal lobe circuits, reducing noise levels and enhancing the specificity of odor representations. Consistently, it was recently reported that pre-exposure to odors recruits dopaminergic neurons, producing latent inhibition in the mushroom body, which leads to changes in fruit fly appetitive behaviors (Jacob et al., 2021). Thus, neuromodulatory systems can help shaping odor representations through local inhibition at different stages in the olfactory processing pathway.

We argue that the sensory-experience-dependent plasticity that we observe in the antennal lobe represents a phenomenon that can be translated to the rest of the brain. This is mainly because such sensory-induced dampening of ongoing neural activity is prominent in many parts of the central nervous system (Raichle, 2010; Raichle et al., 2001). Hence, a sensory-experience-dependent dampening of the internal noise of neural networks can contribute to more effective and specific processing of incoming information. Investigating the presence and mechanisms of this phenomenon is important for understanding how higher brain regions, such as the habenula (Baker et al., 2015; Jetti et al., 2014; Mizumori and Baker, 2017), thalamus (Kirouac, 2015; MacLean et al., 2005), or the cortex (Blaeser et al., 2017; Tan, 2015) contribute to the switching of brain states. Our results revealed that experience-dependent alterations are not only restricted to higher brain regions, but can specifically modulate sensory representations at the first stage of sensory pathways, such as the antennal lobe.

Limitations of the study

Our results highlight that repeated odor experience is important for readjusting the internal dynamics of the olfactory system, and for enhancing the robustness and specificity of odor representations. However, we did not investigate how these processes relate to animal behavior during odor-guided behaviors. Future behavioral studies will be important to understand the behavioral implications of experience-dependent modulation of ongoing and odor-evoked activity. Moreover, we propose that gradual recruitment and facilitation of inhibitory LNs during repeated odor exposure might be a key mechanism underling the experience-dependent plasticity we observed in the fruit fly antennal

lobe. However, we did not investigate the activity of LNs or the neuromodulatory circuits that control the activity of LNs. Further research is needed to elucidate the mechanisms by which inhibitory LNs and neuromodulatory systems are recruited upon repeated odor exposure. Finally, we did not investigate the specific identity of olfactory glomeruli, which prevented us from inspecting whether such experience-dependent plasticity is a feature of distinct antennal glomeruli.

ETHICAL GUIDELINES STATEMENT

All experimental procedures performed were in accordance with the Directive 2010/63/EU of the European Parliament and the Council of the European Union and approved by the Belgian Authorities.

STAR★METHODS

Detailed methods are provided in the online version of this paper and include the following:

- KEY RESOURCES TABLE
- RESOURCE AVAILABILITY
  - Lead contact
  - Materials availability
  - Data and code availability
- EXPERIMENTAL MODEL AND SUBJECT DETAILS
  - *Drosophila melanogaster* maintenance and strains
- METHOD DETAILS
  - Olfactory stimulation
  - Calcium imaging and fly preparation
- QUANTIFICATION AND STATISTICAL ANALYSIS
  - Calcium data postprocessing
  - Ongoing activity analyses
  - Odor-evoked activity analyses
  - Statistical analyses

SUPPLEMENTAL INFORMATION

Supplemental information can be found online at https://doi.org/10.1016/j.celrep.2021.110165.

ACKNOWLEDGMENTS

We thank Ilona Kadow (who shared GH146-GAL4/UAS-GCaMP6m; +/+ flies). This work was funded by VIB (E.Y.), NERF (E.Y.), the VIB International PhD Program (L.M.F.) and ERC Starting Grant 335561 (E.Y). NFR FRIPRO Grant 314212 (E.Y.). The E.Y. lab is funded by the Kavli Institute for Systems Neuroscience at NTNU.

AUTHOR CONTRIBUTIONS

Conceptualization, L.M.F. and E.Y. Methodology, investigation, and analysis, L.M.F. Writing original draft, review, and editing, L.M.F. and E.Y. Funding acquisition, L.M.F. and E.Y. Supervision, E.Y.

DECLARATION OF INTERESTS

The authors declare no competing interests.

INCLUSION AND DIVERSITY

One or more of the authors of this paper self-identifies as an underrepresented ethnic minority in science.

Received: April 28, 2021
Revised: September 10, 2021
Accepted: December 1, 2021
Published: December 28, 2021

REFERENCES

Abraham, N.M., Egger, V., Shimshek, D.R., Renden, R., Fukunaga, I., Sprengel, R., Seeburg, P.H., Klugmann, M., Margrie, T.W., Schaefer, A.T., et al. (2010). Synaptic inhibition in the olfactory bulb accelerates odor discrimination in mice. Neuron *65*, 399–411.

Andalman, A.S., Burns, V.M., Lovett-Barron, M., Broxton, M., Poole, B., Yang, S.J., Grosenick, L., Lerner, T.N., Chen, R., Benster, T., et al. (2019). Neuronal dynamics regulating brain and behavioral state transitions. Cell *177*, 970–985.

Arevian, A.C., Kapoor, V., and Urban, N.N. (2008). Activity-dependent gating of lateral inhibition in the mouse olfactory bulb. Nat. Neurosci. *11*, 80–87.

Arieli, A., Sterkin, A., Grinvald, A., and Aertsen, A. (1996). Dynamics of ongoing activity: explanation of the large variability in evoked cortical responses. Science *273*, 1868–1871.

Baker, P.M., Oh, S.E., Kidder, K.S., and Mizumori, S.J.Y. (2015). Ongoing behavioral state information signaled in the lateral habenula guides choice flexibility in freely moving rats. Front. Behav. Neurosci. *9*, 4.

Banerjee, A., Marbach, F., Anselmi, F., Koh, M.S., Davis, M.B., Garcia da Silva, P., Delevich, K., Oyibo, H.K., Gupta, P., Li, B., et al. (2015). An interglomerular circuit gates glomerular output and implements gain control in the mouse olfactory bulb. Neuron *87*, 193–207.

Bartoszek, E.M., Kumar Jetti, S., Thanh, K., Chau, P., and Yaksi, E. (2021). Ongoing habenular activity is driven by forebrain networks and modulated by olfactory stimuli. Curr. Biol *31*, 3861–3874.e3.

Bazhenov, M., Stopfer, M., Sejnowski, T.J., and Laurent, G. (2005). Fast odor learning improves reliability of odor responses in the locust antennal lobe. Neuron *46*, 483–492.

Berck, M.E., Khandelwal, A., Claus, L., Hernandez-Nunez, L., Si, G., Tabone, C.J., Li, F., Truman, J.W., Fetter, R.D., Louis, M., et al. (2016). The wiring diagram of a glomerular olfactory system. Elife *5*, e14859.

Bhandawat, V., Olsen, S.R., Gouwens, N.W., Schlief, M.L., and Wilson, R.I. (2007). Sensory processing in the Drosophila antennal lobe increases reliability and separability of ensemble odor representations. Nat. Neurosci. *10*, 1474–1482.

Blaeser, A.S., Connors, B.W., and Nurmikko, A.V. (2017). Spontaneous dynamics of neural networks in deep layers of prefrontal cortex. J. Neurophysiol. *117*, 1581–1594.

Boie, S.D., Connor, E.G., McHugh, M., Nagel, K.I., Ermentrout, G.B., Crimaldi, J.P., and Victor, J.D. (2018). Information-theoretic analysis of realistic odor plumes: what cues are useful for determining location? PLoS Comput. Biol. *14*, e1006275.

Boisgontier, M.P., and Cheval, B. (2016). The anova to mixed model transition. Neurosci. Biobehav. Rev. *68*, 1004–1005.

Van Breugel, F., and Dickinson, M.H. (2014). Plume-tracking behavior of flying Drosophila emerges from a set of distinct sensory-motor reflexes. Curr. Biol. *24*, 274–286.

Brill, J., Shao, Z., Puche, A.C., Wachowiak, M., and Shipley, M.T. (2016). Serotonin increases synaptic activity in olfactory bulb glomeruli. J. Neurophysiol. *115*, 1208–1219.

Bundschuh, S.T., Zhu, P., Schärer, Y.P.Z., and Friedrich, R.W. (2012). Dopaminergic modulation of mitral cells and odor responses in the zebrafish olfactory bulb. J. Neurosci. *32*, 6830–6840.

Chen, T.-W., Wardill, T.J., Sun, Y., Pulver, S.R., Renninger, S.L., Baohan, A., Schreiter, E.R., Kerr, R.A., Orger, M.B., Jayaraman, V., et al. (2013). Ultrasensitive fluorescent proteins for imaging neuronal activity. Nature *499*, 295–300.

Chou, Y.-H., Spletter, M.L., Yaksi, E., Leong, J.C.S., Wilson, R.I., and Luo, L. (2010). Diversity and wiring variability of olfactory local interneurons in the Drosophila antennal lobe. Nat. Neurosci. *13*, 439–449.

Christiaens, J.F., Franco, L.M., Cools, T.L., de Meester, L., Michiels, J., Wenseleers, T., Hassan, B.A., Yaksi, E., and Verstrepen, K.J. (2014). The fungal aroma gene ATF1 promotes dispersal of yeast cells through insect vectors. Cell Rep. *9*, 425–432.

Corrales-Carvajal, V.M., Faisal, A.A., and Ribeiro, C. (2016). Internal states drive nutrient homeostasis by modulating exploration-exploitation trade-off. Elife *5*, e19920.

Dacks, A.M., Green, D.S., Root, C.M., Nighorn, A.J., and Wang, J.W. (2009). Serotonin modulates olfactory processing in the antennal lobe of Drosophila. J. Neurogenet. *23*, 366–377.

Das, S., Sadanandappa, M.K., Dervan, A., Larkin, A., Lee, J.A., Sudhakaran, I.P., Priya, R., Heidari, R., Holohan, E.E., Pimentel, A., et al. (2011). Plasticity of local GABAergic interneurons drives olfactory habituation. Proc. Natl. Acad. Sci. U S A *108*, 646–654.

Dugué, G.P., and Mainen, Z.F. (2009). How serotonin gates olfactory information flow. Nat. Neurosci. *12*, 673–675.

Fore, S., Acuña-Hinrichsen, F., Mutlu, K.A., Bartoszek, E.M., Serneels, B., Faturos, N.G., Chau, K.T.P., Cosacak, M.I., Verdugo, C.D., Palumbo, F., et al. (2020). Functional properties of habenular neurons are determined by developmental stage and sequential neurogenesis. Sci. Adv. *6*, eaaz3173.

Fox, M.D., Snyder, A.Z., Vincent, J.L., Corbetta, M., Van Essen, D.C., and Raichle, M.E. (2005). The human brain is intrinsically organized into dynamic, anticorrelated functional networks. Proc. Natl. Acad. Sci. U S A *102*, 9673–9678.

Franco, L.M., and Goard, M.J. (2021). A distributed circuit for associating environmental context with motor choice in retrosplenial cortex. Sci. Adv. *7*, eabf9815.

Franco, L.M., Okray, Z., Linneweber, G.A., Hassan, B.A., and Yaksi, E. (2017). Reduced lateral inhibition impairs olfactory computations and behaviors in a Drosophila model of fragile X syndrome. Curr. Biol. *27*, 1111–1123.

Friedrich, R.W., and Laurent, G. (2004). Dynamics of olfactory bulb input and output activity during odor stimulation in zebrafish. J. Neurophysiol. *91*, 2658–2669.

Fujimoto, S., Leiwe, M.N., Sakaguchi, R., Muroyama, Y., Kobayakawa, R., Kobayakawa, K., Saito, T., and Imai, T. (2019). Spontaneous activity generated within the olfactory bulb establishes the discrete wiring of mitral cell dendrites. BioRxiv. https://doi.org/10.1101/625616.

Galán, R.F., Fourcaud-Trocmé, N., Ermentrout, G.B., and Urban, N.N. (2006a). Correlation-induced synchronization of oscillations in olfactory bulb neurons. J. Neurosci. *26*, 3646–3655.

Galán, R.F., Weidert, M., Menzel, R., Herz, A.V.M., and Galizia, C.G. (2006b). Sensory memory for odors is encoded in spontaneous correlated activity between olfactory glomeruli. Neural Comput. *18*, 10–25.

Giovannucci, A., Friedrich, J., Gunn, P., Kalfon, J., Brown, B.L., Koay, S.A., Taxidis, J., Najafi, F., Gauthier, J.L., Zhou, P., et al. (2019). CaImAn an open source tool for scalable calcium imaging data analysis. Elife *8*, e38173.

Gorin, M., Tsitoura, C., Kahan, A., Watznauer, K., Drose, D.R., Arts, M., Mathar, R., O'Connor, S., Hanganu-Opatz, I.L., Ben-Shaul, Y., et al. (2016). Interdependent conductances drive infraslow intrinsic rhythmogenesis in a subset of accessory olfactory bulb projection neurons. J. Neurosci. *36*, 3127–3144.

Grabe, V., Schubert, M., Strube-Bloss, M., Reinert, A., Trautheim, S., Lavista-Llanos, S., Fiala, A., Hansson, B.S., and Sachse, S. (2020). Odor-induced multi-level inhibitory maps in *Drosophila*. eNeuro *7*. https://doi.org/10.1523/ENEURO.0213-19.2019.

Hahn, T.T.G., McFarland, J.M., Berberich, S., Sakmann, B., and Mehta, M.R. (2012). Spontaneous persistent activity in entorhinal cortex modulates cortico-hippocampal interaction in vivo. Nat. Neurosci. *15*, 1531–1538.

Hsia, A.Y., Vincent, J.-D., and Lledo, P.-M. (1999). Dopamine depresses synaptic inputs into the olfactory bulb. J. Neurophysiol. *82*, 1082–1085.

Ichinose, T., Tanimoto, H., and Yamagata, N. (2017). Behavioral modulation by spontaneous activity of dopamine neurons. Front. Syst. Neurosci. *11*, 88.

Jacob, P.F., Vargas-Gutierrez, P., Okray, Z., Vietti-Michelina, S., Felsenberg, J., and Waddell, S. (2021). An opposing self-reinforced odor pre-exposure memory produces latent inhibition in *Drosophila*. BioRxiv. https://doi.org/10.1101/2021.02.10.430636.

Jacobson, G.A., Rupprecht, P., and Friedrich, R.W. (2018). Experience-dependent plasticity of odor representations in the telencephalon of zebrafish. Curr. Biol. *28*, 1–14.

Jetti, S.K., Vendrell-Llopis, N., and Yaksi, E. (2014). Spontaneous activity governs olfactory representations in spatially organized habenular microcircuits. Curr. Biol. *24*, 434–439.

Kazama, H., and Wilson, R.I. (2009). Origins of correlated activity in an olfactory circuit. Nat. Neurosci. *12*, 1136–1144.

Kilgard, M.P., and Merzenich, M.M. (1998). Cortical map reorganization enabled by nucleus basalis activity. Science *279*, 1714–1718.

Kirouac, G.J. (2015). Placing the paraventricular nucleus of the thalamus within the brain circuits that control behavior. Neurosci. Biobehav. Rev. *56*, 315–329.

Koerner, T.K., and Zhang, Y. (2017). Application of linear mixed-effects models in human neuroscience research: a comparison with Pearson correlation in two auditory electrophysiology studies. Brain Sci. *7*, 26.

Lange, R.D., and Haefner, R.M. (2017). Characterizing and interpreting the influence of internal variables on sensory activity. Curr. Opin. Neurobiol. *46*, 84–89.

Lewis, S.M., Xu, L., Rigolli, N., Tariq, M.F., Stern, M., Seminara, A., and Gire, D.H. (2020). Plume dynamics structure the spatiotemporal activity of glomerular networks in the mouse olfactory bulb. BioRxiv. https://doi.org/10.1101/2020.11.25.399089.

Liu, S. (2020). Dopamine suppresses synaptic responses of fan cells in the lateral entorhinal cortex to olfactory bulb input in mice. Front. Cell. Neurosci. *14*, 181.

Lottem, E., Lörincz, M.L., and Mainen, Z.F. (2016). Optogenetic activation of dorsal raphe serotonin neurons rapidly inhibits spontaneous but not odor-evoked activity in olfactory cortex. J. Neurosci. *36*, 7–18.

Louis, M., Huber, T., Benton, R., Sakmar, T.P., and Vosshall, L.B. (2008). Bilateral olfactory sensory input enhances chemotaxis behavior. Nat. Neurosci. *11*, 187–199.

Lovett-Barron, M., Andalman, A.S., Allen, W.E., Vesuna, S., Kauvar, I., Burns, V.M., and Deisseroth, K. (2017). Ancestral circuits for the coordinated modulation of brain state. Cell *171*, 1411–1423.

MacLean, J.N., Watson, B.O., Aaron, G.B., and Yuste, R. (2005). Internal dynamics determine the cortical response to thalamic stimulation. Neuron *48*, 811–823.

Marques, J.C., Li, M., Schaak, D., Robson, D.N., and Li, J.M. (2020). Internal state dynamics shape brainwide activity and foraging behaviour. Nature *577*, 239–243.

Mizumori, S.J.Y., and Baker, P.M. (2017). The lateral habenula and adaptive behaviors. Trends Neurosci. *40*, 481–493.

Mukamel, E.A., Nimmerjahn, A., and Schnitzer, M.J. (2009). Automated analysis of cellular signals from large-scale calcium imaging data. Neuron *63*, 747–760.

Musall, S., Kaufman, M.T., Juavinett, A.L., Gluf, S., and Churchland, A.K. (2019). Single-trial neural dynamics are dominated by richly varied movements. Nat. Neurosci. *22*, 1677–1686.

Nagel, K.I., and Wilson, R.I. (2016). Mechanisms underlying population response dynamics in inhibitory interneurons of the *Drosophila* antennal lobe. J. Neurosci. *36*, 4325–4338.

Nagel, K.I., Hong, E.J., and Wilson, R.I. (2015). Synaptic and circuit mechanisms promoting broadband transmission of olfactory stimulus dynamics. Nat. Neurosci. *18*, 56–65.

Olsen, S.R., and Wilson, R.I. (2008). Lateral presynaptic inhibition mediates gain control in an olfactory circuit. Nature *452*, 956–960.

Olsen, S.R., Bhandawat, V., and Wilson, R.I. (2010). Divisive normalization in olfactory population codes. Neuron *66*, 287–299.

Padmanabhan, K., and Urban, N.N. (2010). Intrinsic biophysical diversity decorrelates neuronal firing while increasing information content. Nat. Neurosci. *13*, 1276–1282.

Park, I.J., Hein, A.M., Bobkov, Y.V., Reidenbach, M.A., Ache, B.W., and Principe, J.C. (2016). Neurally encoding time for olfactory navigation. PLoS Comput. Biol. *12*, e1004682.

Petzold, G.C., Hagiwara, A., and Murthy, V.N. (2009). Serotonergic modulation of odor input to the mammalian olfactory bulb. Nat. Neurosci. *12*, 784–791.

Poort, J., Khan, A.G., Pachitariu, M., Nemri, A., Orsolic, I., Krupic, J., Bauza, M., Sahani, M., Keller, G.B., Mrsic-Flogel, T.D., et al. (2015). Learning enhances sensory and multiple non-sensory representations in primary visual cortex. Neuron *86*, 1478–1490.

Popov, T., and Szyszka, P. (2020). Alpha oscillations govern interhemispheric spike timing coordination in the honey bee brain. Proc. R. Soc. B Biol. Sci. *287*, 20200115.

Porter, J., Craven, B., Khan, R.M., Chang, S.J., Kang, I., Judkewitz, B., Volpe, J., Settles, G., and Sobel, N. (2007). Mechanisms of scent-tracking in humans. Nat. Neurosci. *10*, 27–29.

Raichle, M.E. (2010). Two views of brain function. Trends Cogn. Sci. *14*, 180–190.

Raichle, M.E., MacLeod, A.M., Snyder, A.Z., Powers, W.J., Gusnard, D.A., and Shulman, G.L. (2001). A default mode of brain function. Proc. Natl. Acad. Sci. U S A *98*, 676–682.

Rein, J., Mustard, J.A., Strauch, M., Smith, B.H., and Galizia, C.G. (2013). Octopamine modulates activity of neural networks in the honey bee antennal lobe. J. Comp. Physiol. A Neuroethol. Sens. Neural Behav. Physiol. *199*, 947–962.

Reiten, I., Uslu, F.E., Fore, S., Pelgrims, R., Ringers, C., Diaz Verdugo, C., Hoffman, M., Lal, P., Kawakami, K., Pekkan, K., et al. (2017). Motile-cilia-mediated flow improves sensitivity and temporal resolution of olfactory computations. Curr. Biol. *27*, 166–174.

Rojas-Líbano, D., Frederick, D.E., Egaña, J.I., and Kay, L.M. (2014). The olfactory bulb theta rhythm follows all frequencies of diaphragmatic respiration in the freely behaving rat. Front. Behav. Neurosci. *8*, 214.

Romano, S.A., Pietri, T., Pérez-Schuster, V., Jouary, A., Haudrechy, M., and Sumbre, G. (2015). Spontaneous neuronal network dynamics reveal circuit's functional adaptations for behavior. Neuron *85*, 1070–1085.

Romano, S.A., Pérez-Schuster, V., Jouary, A., Boulanger-Weill, J., Candeo, A., Pietri, T., and Sumbre, G. (2017). An integrated calcium imaging processing toolbox for the analysis of neuronal population dynamics. PLoS Comput. Biol. *13*, e1005526.

Root, C.M., Masuyama, K., Green, D.S., Enell, L.E., Nässel, D.R., Lee, C.H., and Wang, J.W. (2008). A presynaptic gain control mechanism fine-tunes olfactory behavior. Neuron *59*, 311–321.

Sachse, S., Rueckert, E., Keller, A., Okada, R., Tanaka, N.K., Ito, K., and Vosshall, L.B.B. (2007). Activity-dependent plasticity in an olfactory circuit. Neuron *56*, 838–850.

Sadaghiani, S., Hesselmann, G., Friston, K.J., and Kleinschmidt, A. (2010). The relation of ongoing brain activity, evoked neural responses, and cognition. Front. Syst. Neurosci. *4*, 20.

Shimaoka, D., Steinmetz, N.A., Harris, K.D., and Carandini, M. (2019). The impact of bilateral ongoing activity on evoked responses in mouse cortex. Elife *8*, e43533.

Stopfer, M., and Laurent, G. (1999). Short-term memory in olfactory network dynamics. Nature *402*, 664–668.

Tabor, R., Yaksi, E., and Friedrich, R.W. (2008). Multiple functions of $GABA_A$ and $GABA_B$ receptors during pattern processing in the zebrafish olfactory bulb. Eur. J. Neurosci. *28*, 117–127.

Tan, A.Y.Y. (2015). Spatial diversity of spontaneous activity in the cortex. Front. Neural Circuits *9*, 48.

Vanni, M.P., and Murphy, T.H. (2014). Mesoscale transcranial spontaneous activity mapping in GCaMP3 transgenic mice reveals extensive reciprocal connections between areas of somatomotor cortex. J. Neurosci. *34*, 15931–15946.

Vickers, N.J., Christensen, T.A., Baker, T.C., and Hildebrand, J.G. (2001). Odour-plume dynamics influence file brain's olfactory code. Nature *410*, 466–470.

Victor, J.D., Boie, S.D., Connor, E.G., Crimaldi, J.P., Ermentrout, G.B., and Nagel, K.I. (2019). Olfactory navigation and the receptor nonlinearity. J. Neurosci. *39*, 3713–3727.

Wilson, D.A., and Yan, X. (2010). Sleep-like states modulate functional connectivity in the rat olfactory system. J. Neurophysiol. *104*, 3231–3239.

Wilson, R.I., and Laurent, G. (2005). Role of GABAergic inhibition in shaping odor-evoked spatiotemporal patterns in the *Drosophila* antennal lobe. J. Neurosci. *25*, 9069–9079.

Wosniack, M.E., Kirchner, J.H., Chao, L.-Y., Zabouri, N., Lohmann, C., and Gjorgjieva, J. (2021). Adaptation of spontaneous activity in the developing visual cortex. Elife *10*, e61619.

Yaksi, E., and Friedrich, R.W. (2006). Reconstruction of firing rate changes across neuronal populations by temporally deconvolved Ca2+ imaging. Nat. Methods *35*, 377–383.

STAR★METHODS

KEY RESOURCES TABLE

REAGENT or RESOURCE	SOURCE	IDENTIFIER
Chemicals, peptides, and recombinant proteins		
1-pentanol	Sigma-Aldrich	138975
2-heptanone	Sigma-Aldrich	537683
3-octanol	Sigma-Aldrich	218405
4-methylcyclohexanol	Sigma-Aldrich	153095
amyl acetate	Sigma-Aldrich	109584
Benzaldehyde	Sigma-Aldrich	418099
ethyl acetate	Sigma-Aldrich	270989
ethyl valerate	Sigma-Aldrich	290866
Sodium chloride (NaCl)	Sigma-Aldrich	S5886
Potassium chloride (KCl)	Sigma-Aldrich	P5405
Sodium phosphate monobasic (NaH_2PO_4)	Sigma-Aldrich	S5011
Calcium chloride ($CaCl_2$)	Sigma-Aldrich	C5670
Magnesium chloride ($MgCl_2$)	Sigma-Aldrich	M4880
Sodium bicarbonate ($NaHCO_3$)	Sigma-Aldrich	S5761
TES	Sigma-Aldrich	T5691
Glucose	Sigma-Aldrich	G7021
Trehalose	Sigma-Aldrich	T0167
Deposited data		
Calcium imaging data are openly available	Dryad	https://doi.org/10.25349/D95S4J
Experimental models: Organisms/strains		
Drosophila melanogaster: y^1w^{1118};;GH146-GAL4;	Bloomington Drosophila Stock Center	BDSC: 30026
Drosophila melanogaster: y^1w^{1118};;UAS-GCaMP6m;	Bloomington Drosophila Stock Center	BDSC: 42748
Software and algorithms		
MATLAB	Mathworks	R2016b
MATLAB codes are openly available	Dryad	https://doi.org/10.5281/zenodo.5781453
Other		
EM-CCD camera	Hamamatsu Photonics	ImagEM X2
Fluorescence microscope	Olympus Corporation	Olympus BX51

RESOURCE AVAILABILITY

Lead contact

Further information and requests for resources and reagents should be directed to and will be fulfilled by the lead contact, Emre Yaksi (emre.yaksi@ntnu.no)

Materials availability

This study did not generate new unique reagents.

Data and code availability

All data have been deposited in Dryad and are publicly available as of the date of publication. DOI is listed in the key resources table.

All original code has been deposited in Zenodo and is publicly available as of the date of publication. DOI is listed in the key resources table.

Any additional information required to reanalyze the data reported in this article is available from the lead contact upon request.

EXPERIMENTAL MODEL AND SUBJECT DETAILS

Drosophila melanogaster maintenance and strains

GH146-GAL4/UAS-GCaMP6m; +/+ *D melanogaster* strains (kindly provided by Ilona Kadow) were raised on standard cornmeal/agar medium supplemented with dry yeast at 25°C with a 12-h light/dark cycle.

METHOD DETAILS

Olfactory stimulation

Odors for protocol 1 (Figures 1, 2, and S1–S7) are 1-pentanol, 2-heptanone, 3-octanol, 4-methylcyclohexanol, amyl acetate, benzaldehyde, ethyl acetate, and ethyl valerate. Odors for protocol 2 (Figure 3 and S8) are ethyl acetate (repeated) and benzaldehyde (unrepeated). All odors were diluted 1:100 v/v in paraffin oil. Odors were delivered through a custom-built mechanism that dilutes the headspace of the odor vial a further 10-fold in clean air. The flow rate of odor delivery was 2.2 L/min. Odors were applied for 500 ms, either 8 times (protocol 1) or 5 times (protocol 2) per train of stimuli, with an intertrial interval of 15 s. Each train of stimuli was spaced by 6 min (protocol 1) or 10 min (protocol 2) where no odor stimulation was applied. The stimulation protocol was controlled by a Master-8 stimulator (A.M.P.I.), programmed for each protocol, respectively.

Calcium imaging and fly preparation

Calcium imaging experiments were conducted on 5- to 10-day posteclosion females; GH146-GAL4/UAS-GCaMP6m; +/+ flies. For each experiment, a fly was secured to a custom chamber made of aluminum foil, smoothly shaped to fit the thorax and the upper part of the head. The fly was then fixed to the chamber with wax, surrounding the space between the fly and the top of the chamber. Also, the front and middle legs as well as the proboscis were carefully immobilized with small drops of wax to the bottom of the chamber. Next, the cuticle above the antennal lobes was carefully removed using a very sharp needle made of tungsten wire. The dorsal side of the antennal lobes was then imaged while constantly perfusing the brain with oxygenated saline. The saline contained (in mM): 103 NaCl, 3 KCl, 1 NaH_2PO_4, 1.5 $CaCl_2$, 4 $MgCl_2$, 26 $NaHCO_3$, 5 TES, 10 glucose, and 8 trehalose. GCaMP6m fluoresce was imaged at 10 Hz using an EMCCD camera (Hamamatsu Photonics) installed on an Olympus BX51 fluorescence microscope (Olympus Corporation).

QUANTIFICATION AND STATISTICAL ANALYSIS

Calcium data postprocessing

Fluorescence imaging stacks were processed using custom code written in MATLAB (MathWorks). Briefly, an independent component analysis was performed on raw fluorescence stacks corresponding with the left and to right antennal lobes, respectively, for each experimental session (Franco et al., 2017; Mukamel et al., 2009). The resulting independent components were then manually curated to eliminate noisy components corresponding with either artifacts in the surrounding of the antennal lobes, or very small regions, likely arising from noisy pixels. This procedure yields a map containing clusters of pixels with similar fluorescence variability, corresponding with functional glomeruli (Figure 1B).

To obtain the activity time series for each glomerulus, we first processed raw fluorescence stacks on a pixel-by-pixel basis, defining a moving F0 as the lowest 10th percentile (Giovannucci et al., 2019; Romano et al., 2017) over a 30-s sliding window, centered around each time bin, which was then used to calculate the $\Delta F/F$ for each time bin. Next, we averaged the activity time series for all pixels contained in the region described by each corresponding glomerulus. The resulting glomerulus time series were used for all subsequent analyses.

Ongoing activity analyses

Ongoing activity across glomeruli was compared by computing the Pearson's correlation coefficient on the entire 6 min (protocol 1) or 10 min (protocol 2) traces for all glomeruli pairs and all epoch pairs corresponding to each experimental session. Similarly, k-mean clustering was performed on the full ongoing activity traces from each epoch. When assigning glomeruli into clusters, the distances between individual glomerulus were calculated based on the cosine distances between their ongoing activity. Cluster fidelity was measured as the probability of a particular glomerulus staying in the same cluster for different epochs. As a control, we shuffled cluster identity of individual glomeruli and performed the calculation again.

For the detection of ongoing calcium events during recording of ongoing activity, we identified the local maxima along each activity trace, setting the minimum width to 1 s, the maximum width to 10 s, and the minimum amplitude threshold to 3 $\Delta F/F$.

Odor-evoked activity analyses

Odor responses were defined as the average activity during a 1.5-s window after response onset for each glomerulus. This window corresponds with the rising phase and initial decay of the odor response, which reflects the underlaying firing rate change (Chen et al., 2013; Yaksi and Friedrich, 2006).

To evaluate the similarity across activity patterns elicited in the antennal lobe by odor stimulation, we constructed odor vectors consisting of odor responses from all glomeruli for each experimental session. We then used the Pearson's correlation coefficient and Euclidean distances to compare across odor vectors. In addition, we calculated the population sparseness as:

$$S = \frac{1 - \frac{\left(\sum \frac{r_i^2}{2}\right)}{\sum \left(\frac{r_i^2}{2}\right)}}{1 - \frac{1}{n}}$$

where r_i is the response of the ith glomerulus to a particular odor and n is the total number of glomeruli per fly. Values near 0 indicate low selectivity, whereas values near 1 indicate high selectivity of the antennal lobe circuit for a particular odor.

Statistical analyses

All data groups were compared using a linear mixed-effects model with a restricted maximum likelihood (Boisgontier and Cheval, 2016; Franco and Goard, 2021; Koerner and Zhang, 2017), except when noted otherwise. Linear mixed-effects models consider both the nested (multiple observations within a single fly/odor for a particular stimulus/train) and crossed (flies/odors observed across multiple stimuli/trains) structure of the data. Thus, by treating flies and odors as random effects, and stimuli and trains as fixed effects, our results comparing odor stimuli and trains can be generalized to the population of flies and to the population of odors. Significant statistical differences are shown either by an asterisk or by color in p-value matrices, as indicated in the figures. Specific p-values are described in figure legends. All analyses were performed using custom code written in Matlab (MathWorks).